CONFERENCE PRE-PRINT

OVERVIEW OF THE KSTAR EXPERIMENTS AND FUTURE PLAN

Y. U. NAM
Korea Institute of Fusion Energy
Daejeon, Republic of Korea
Email: yunam@kfe.re.kr

H. HAN, H.H. LEE, J. CHUNG, Y.M. JEON, G.Y. PARK, J. KIM, K. KIM, M. KIM, J. KO, S. WANG, J. LEE, S.-H. HAHN, H.S. KIM, J.W. JUHN, J. LEE, W.H. KO, G. SHIN, Y. LEE, J.K. LEE, B. KIM, S. HONG, Y.S. PARK, J.G. BAK, M.J. CHOI, M. JOUNG, J.S. KANG, J.H. JEONG, S.G. LEE, B.H. PARK, J.H. LEE, K.D. LEE, E.N. BANG, H.S. KIM, C.S. BYUN, S.T. OH, S.H. SON, H.M.WI, D.C. SEO, J.H. JANG, S.H. PARK, S. KWON, S.W. KWAG, H.T. KIM, Y.B. CHANG, N.H. SONG, M.K. KIM, K.P. KIM, C.R. SEON, J.I. SONG, S.H. PARK, H.M. LEE, Y.O. KIM, I.S. WOO, W. CHO, J.S. KIM, H. KIM, J.G. KWAK, W.C. KIM, S.W. YOON and the KSTAR Team
Korea Institute of Fusion Energy
Daejeon, Republic of Korea

K. LEE, G.H. PARK, J. KO
Korean University of Science and Technology
Daejeon, Republic of Korea

Y.-C. GHIM, C. SUNG, J.H. HWANG, D. KIM, Y.S. HAN, H.Y. JEONG, C.Y.LEE, J.-s. LEE, W.H. CHOE
Korea Advanced Institute of Science and Technology
Daejeon, Republic of Korea

Y.S. NA, J.-K. PARK, W. JEONG, Y.S. HWANG
Seoul National University
Seoul, Republic of Korea

S.K. KIM, Q.M. HU, S.M. YANG, E. KOLEMEN, K. ERICKSON, R. SHOUSHA, J. YOO, C.S. BYUN, H. SCHAMIS, E. GILSON, J.H. YOON, S.M. BONG, R. MAINGI
Princeton Plasma Physics Laboratory
Princeton, USA

J.M. PARK, K. Kim
Oak Ridge National Laboratory
Oak Ridge, USA

S. DING, H.Q. WANG, A.M. GAROFALO, D. ELDON, A. GUPTA, J. BARR, A. THORNTON, S. HONG, K.B. KWON, A. NAGY, A. BORTOLON
General Atomics
San Diego, USA

K. KWON
Oak Ridge Associated University
Tennessee, USA

S.A. SABBAGH, G. BUSTOS-RAMIREZ, J.D. RIQUEZES, M. TOBIN, H. LEE, F.C. SHEEHAN, V. ZAMKOVSKA, J.R. JEPSON, G.A. TILLINGHAST
Columbia University
New York, USA

E. KIM
Coventry University, Coventry
United Kingdom

C. HAM, A. KIRK, L. KOGAN, D. RYAN, B. PATEL

United Kingdom Atomic Energy Authority
Abingdon, United Kingdom

S.H. KIM, R.A. PITTS, A.A. PSHENOV
ITER Organization
Cadarache, France

H. LEE, J. LEE
Hanyang University
Seoul, Republic of Korea

Y.G. LIM
California Institute of Technology
California, USA

V. ALARCON, F. LAGGNER
North Carolina State University
North Carolina, USA

Abstract

The Korea Superconducting Tokamak Advanced Research (KSTAR) device has recently entered a new phase of operation following the installation of a tungsten mono-block divertor, providing a unique platform to investigate high-performance, long-pulse plasma scenarios for future reactors. The 2023–2024 experimental campaigns demonstrated significant progress in commissioning the tungsten divertor, developing plasma operation scenarios, and achieving real-time control. Comparative studies revealed increased core radiation losses and associated performance degradation relative to the carbon divertor environment. Mitigation strategies, such as optimized neutral beam injection timing, boron powder seeding, and impurity control through gas puffing, were shown to reduce tungsten accumulation and extend high-performance phases, including record H-mode operation exceeding 100 s. Collaborative development with DIII-D enabled the first demonstration of high poloidal beta scenarios with an internal transport barrier on KSTAR. Advances in control included upgraded real-time resonant magnetic perturbation schemes and disruption forecasting via the DECAF system. Furthermore, divertor detachment control using a new surrogate-model-based approach with real-time radiation imaging demonstrated active impurity and heat flux management. Supported by enhanced heating, current drive, and diagnostic systems, these achievements offer valuable insights into tungsten impurity behavior, transport physics, and control strategies for future reactors including ITER. Planned upgrades toward a full-tungsten wall and ITER-aligned real-time plasma control will further establish KSTAR as a leading experimental platform for developing operational scenarios required to achieve steady-state, burning plasma conditions.

1. INTRODUCTION

KSTAR is a superconducting tokamak capable of high-performance long-pulse experiments with recently equipped tungsten (W) mono-block divertor. KSTAR project aims to develop high-performance operation scenarios for the demonstration reactor including control schemes to avoid critical events relating plasma instabilities [1,2]. The new W divertor has provided a unique opportunity to investigate impurity transport and plasma–wall interactions under reactor-relevant conditions. Tungsten, chosen as the primary divertor material for ITER and DEMO, offers superior thermo-mechanical resilience but introduces severe radiative risks due to its high atomic number. Even accumulation of W in the core plasma can substantially enhance radiation losses and deteriorate plasma confinement, making impurity control one of the central challenges in present and future devices. The 2023-2024 KSTAR campaign focused on deploying the new W mono-block diverter cassette to validate plasma operations similar to previous seasons with a full carbon wall.

The main mission of KSTAR is to develop plasma operation scenarios applicable to the burning plasma stage. To enhance the economic viability of the commercial reactor and accelerate the realization of net electricity generation, it is necessary to achieve high-performance, steady-state fusion reactions in smaller fusion reactors while minimizing the support of external heating and current drive devices. This requires operating scenarios with superior confinement performance and self-current driving capabilities compared to conventional H-mode scenarios, as well as control techniques that can effectively suppress various instabilities and harmful events. KSTAR will verify the performance of advanced operation scenarios and their applicability to demonstration reactors through long-pulse operations in a W environment. KSTAR will also test methods to enhance core plasma performance and stability by introducing cutting-edge control techniques, including artificial intelligence. Furthermore, KSTAR will explore innovative approaches to improve confinement performance based on a deep

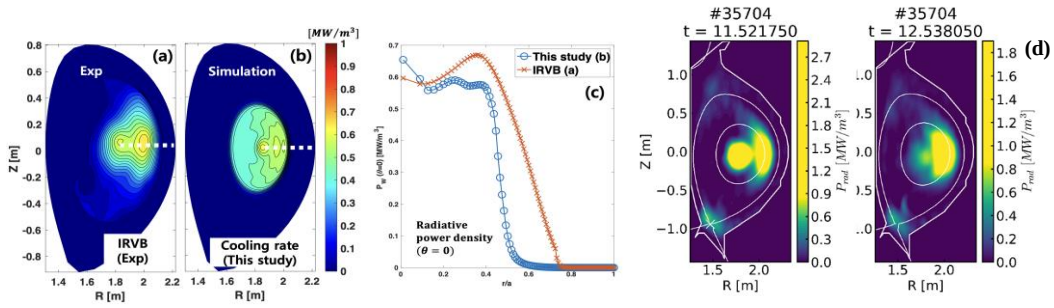

FIG 1. Comparison of heating schemes in tungsten divertor plasmas. (a) gradual ramp-up of heating leads to significant increase in core radiation (P_{rad} ~ 2 MW). (b) β-kicking NBI heating substantially reduces core radiation (P_{rad} ~ 0.14 MW) while improving confinement (H_{89} ~ 1.7). Potential impacts of low-Z seeded impurities on the high-Z impurity transport in ITER-relevant case (d) 2D radiation map was also modified during the Ne injection

understanding of the physical mechanisms of transport and instability phenomena in tokamak burning plasma environments.

2. SUPPRESSION OF TUNGSTEN IMPURITIES

After installation of new divertor, key adjustments were made to plasma startup and shape control considering the up-down asymmetry configuration. The currents on the poloidal field coil in the startup phase and the striking target point on the divertor plate during shaping phase are adjusted to compensate for the asymmetry. In addition, visible spectrometry and bolometry were used to study W atom generation and transport, including experiments with noble gas injection into the divertor. These efforts provided valuable insights into the behavior of W in the plasma and its impact on divertor performance, laying the groundwork for future improvements in the next campaign.

The deleterious effects of W impurities were confirmed through systematic comparisons of plasma operation with lower single-null (LSN, W divertor target) and upper single-null (USN, carbon divertor target) discharges. Two-dimensional radiation loss profiles from the infrared video bolometer (IRVB) revealed pronounced core radiation following the introduction of the W divertor, while USN plasmas on graphite targets showed no significant central radiation. A tungsten impurity transport simulation, employing neoclassical (FACIT) and turbulent (TGLF) transport models along with strong rotation effects [3], enables estimation of the tungsten distribution. FIG 1 shows comparison between the IRVB data and the reconstructed tungsten cooling rate based on the simulations for KSTAR H-mode discharge. The analysis indicates that the maximum tungsten density in KSTAR inferred from the total radiative power is approximately 400-500 times lower than the main ion density. Dedicated experiments investigated the potential impacts of low-Z seeded impurities on the high-Z impurity transport [4], employing Kr as the ITER-relevant high-Z impurity proxy for tungsten and Ne as the low-Z seeded impurity for ITER. Kr injection into the target background plasma with a very low content of tungsten impurities increased the core radiative power loss fraction up to 30%, similarly to the ITER radiative core conditions and the edge pedestal with mitigated small ELMs. Ne was injected to assess the response of the core impurities and radiative power loss, which decreased total radiative power loss slowly and the centrally peaked radiation moved off-axis. The experimental results imply that additional Kr influx through the (mitigated) plasma pedestal or Kr is moved off-axis where the temperature is lower. 2D radiation map was also modified during the Ne injection, indicating that there are non-linear processes that require dedicated modelling activities (FIG 1(d)). These findings emphasize critical need for impurity avoidance and mitigation strategies in W divertor environments.

To address W accumulation, new plasma operation scenarios were developed. A particularly effective method is the β-kicking neutral beam heating scenario, in which most of the NBI power is applied only after the plasma has entered H-mode and magnetic shape control has been secured. By delaying strong auxiliary heating and imposing a deuterium gas puff near the divertor, initial W sputtering is minimized, significantly reducing subsequent impurity penetration. Experiments demonstrated that plasmas operated under this scheme exhibited enhanced pedestal stability, reduced core radiation, and improved confinement compared with conventional NBI timing. Another key approach has been the application of boron powder injection using the impurity powder dropper (IPD). Boronization was found to remain effective even under H-mode plasmas with the W divertor, suppressing both total and core radiation losses [5]. IRVB measurements confirmed that cumulative boron injection led to a redistribution of radiated power away from the plasma core. These results establish IPD boronization as a

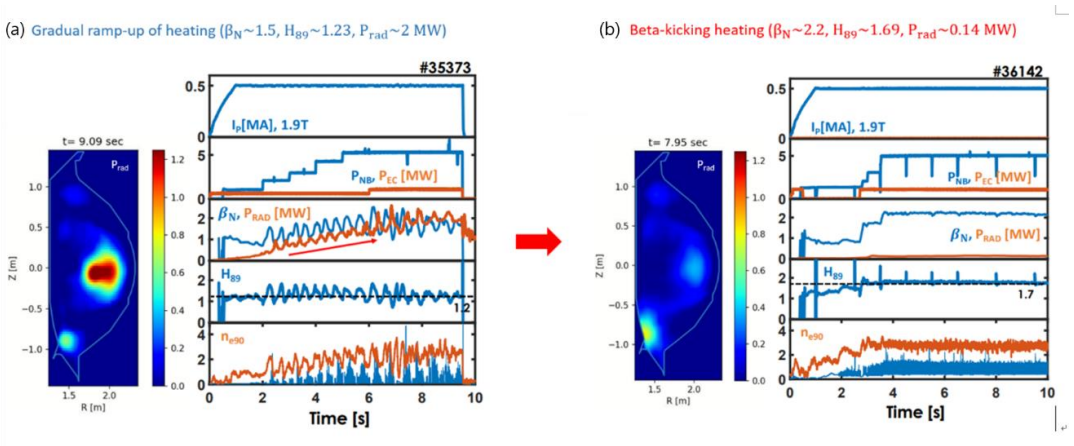

FIG 2. Comparison of heating schemes in W divertor plasmas. (a) gradual ramp-up of heating leads to significant increase in core radiation (P_{rad} ~ 2 MW). (b) β-kicking NBI heating substantially reduces core radiation (P_{rad} ~ 0.14 MW) while improving confinement (H_{89} ~ 1.7).

repeatable wall conditioning technique that complements traditional glow discharge cleaning and electron cyclotron wall conditioning.

3. ADVANCED SCENARIO DEVELOPMENT

Until the 2022 campaign, various candidate scenarios were developed in a full-carbon environment, including high-β_p, high-l_i, hybrid, ITB, FIRE, and I-mode, with a focus on high plasma pressure and confinement [6-10]. Significant milestones were achieved, such as the establishment of a hot-ion scenario where the central ion temperature exceeded 9 keV for up to 30 s, and a high-l_i discharge sustaining β_N ~ 3 for 12 s in an USN configuration. Additionally, studies explored triggering coherent edge-localized modes [11] and transitioning from LSN to double null (DN) configurations [12] to enhance β_N in the hybrid scenario. The new W divertor has been particularly beneficial for long-pulse LSN scenarios though USN scenarios face challenges due to the mixed carbon-tungsten environment [13]. The 2023-2024 campaigns prioritized evaluating these effects, and the W divertor commissioning builds on these efforts by examining the performance and stability limits of these scenarios in the new W environment.

The high-l_i scenario, designed for high-β_N operation [6], was successfully reproduced at β_N ~ 3 for ~10 s in the 2023 campaign as shown in FIG 3. Plasma shapes were consistent with 2022 references, and increased flexibility in neutral beam (NB) heating allowed better control of the β_N ramp rate through the upgraded NB2 feedforward power control system. This capability mitigated performance overshoots and MHD instabilities often caused by rapid β_N rise during beam injection. Supplemental electron cyclotron (EC) heating was also used as a regulator to stabilize β_N evolution. While robust operation was demonstrated during the early discharge phase, performance degradation was observed after 13 s. No major MHD activity was observed, but enhanced radiation near the X-point and impurity influx from the outer divertor region correlated with reductions in T_e, increases in loop voltage, and rising n_e, consistent with radiation-driven confinement degradation. To improve

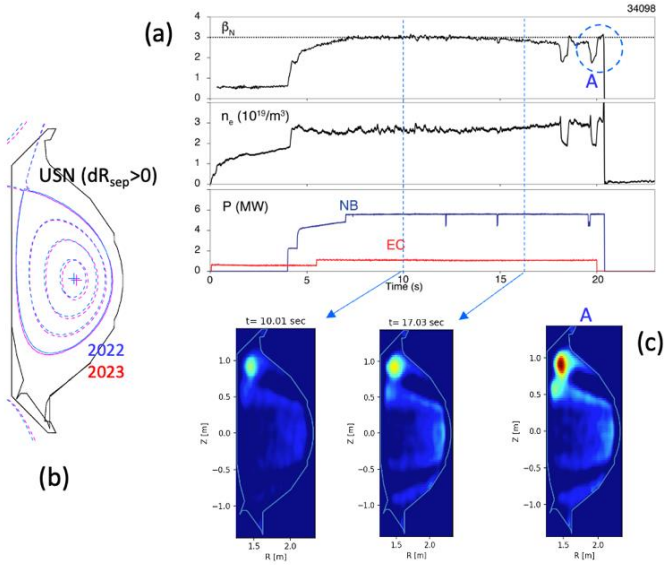

FIG 3. The High-l_i scenario reproduced β_N ~ 3 operation after the lower W divertor modification (a). Plasma shapes were consistent for the upper single-null configuration (b), with strong radiation near the upper X-point observed in the long pulse operation (c).

compatibility with the W divertor, a double-null version of the high-l_i scenario was also developed. After reproducing the upper single-null reference discharge, the plasma shape was transitioned toward a near double-null configuration. Despite a sudden radiation increase following the transition, $\beta_N \sim 2.8$ was maintained, demonstrating a

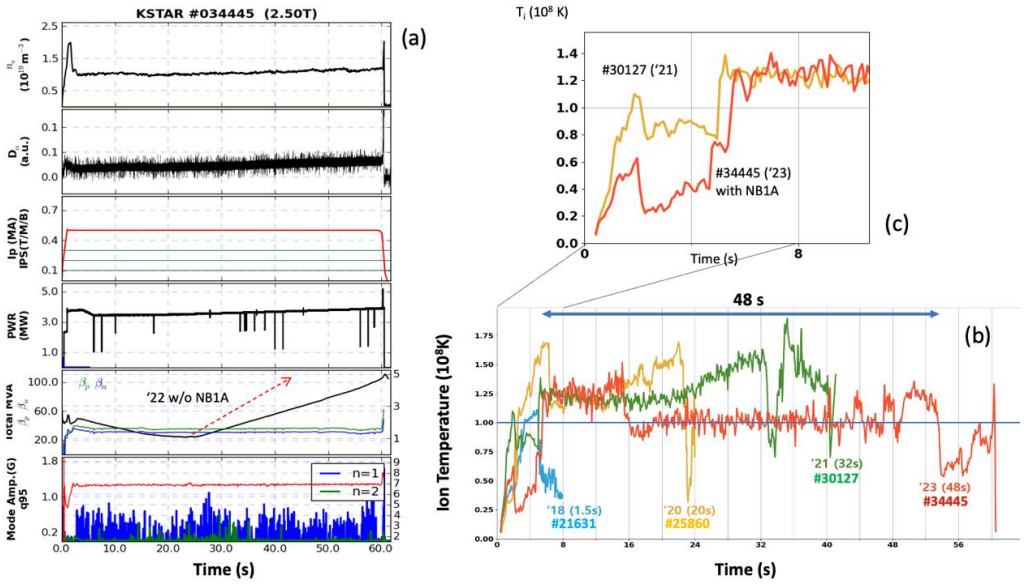

FIG 4. Reproduced FIRE-mode discharge lasting 60 s (a), with T_i above 10^8 K sustained for 48 s (b) using an optimized beam ramp-up to avoid T_i overshoot at the beginning of discharge (c).

potential path to W-compatible high-β_N operation.

High ion-temperature (high-T_i) operation, based on the FIRE mode [9], employs upper single-null plasmas at relatively low electron density ($n_e < 1.5 \times 10^{19}$ m^{-3}). In 2023, this regime was extended to 48 s in the W environment as shown in FIG 4. A representative discharge lasted 60 s at $B_T = 2.5$ T and $I_p = 500$ kA, with carefully optimized beam ramp-up to balance increasing density while avoiding MHD instabilities. Higher toroidal field operation enabled higher NB power consistent with the elevated L-H threshold, lowering loop voltage and conserving poloidal flux both crucial for long-pulse operation under PF coil power-supply limitations. Beam shine-through, which can cause localized wall heating, was actively managed. Attempts to increase density for reduced beam shine-through included additional gas fueling, supersonic molecular beam injection (SMBI), higher I_p, and application of edge-resonant magnetic perturbations (ERMP). However, these approaches did not yield H-mode transitions except in limited configurations. At higher B_T, increased density was achieved, albeit with reduced energy confinement.

The hybrid scenario, characterized by enhanced edge stability and core confinement [7], was pursued in the W divertor with emphasis on extending pulse duration. In the W environment, a new reference hybrid scenario was established with plasma shape and q_{95} comparable to the previous reference. Divertor gas puffing at 1.5 s reduced W influx, while I_p was increased in two steps to ensure stable L–H transition. This

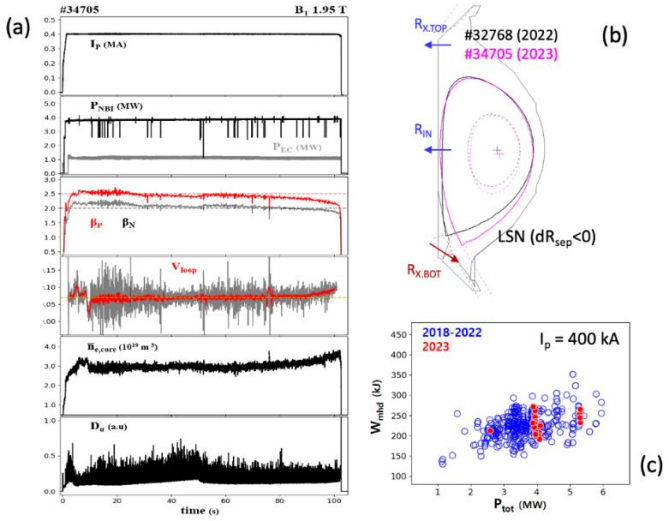

FIG 5. A 102 s high-performance long-pulse was achieved (a). The lower single-null plasma shape was adopted to the new W divertor (b), and the overall plasma performance in the new environment was observed to be similar in the operation regime at I_p = 400 kA (c).

configuration achieved β_N ~ 2.6 for ~2.5 s, before the density increases from main gas fueling reduced performance.

Pulse length of the H-mode extended significantly, with a 102 s lower single-null H-mode discharge at I_p = 400 kA and total injected power of 5 MW. The discharge sustained $\beta_N > 2.0$ with minimal performance degradation up to 70 s as shown in FIG 5. Technical improvements included mitigation of measurement drift and reduced PFC temperature excursions (<15 °C). These results validate the W divertor upgrade for long-pulse operation. However, achieving the ~ 300 s pulse requires fully non-inductive operation and hardware upgrades.

Enhanced initial magnetization was tested as a means to support higher I_p and plasma volume, with new control schemes enabling >40% higher initial magnetic flux. This approach is expected to extend pulse length by ~15 s, although further hardware development is necessary. Exploratory studies of negative-triangularity plasmas were conducted using feedforward control, achieving partial isoflux control despite challenges with ECH requirements and RT-EFIT. Dedicated campaigns are planned for further optimization. Startup in reversed toroidal field was also investigated. Initial attempts were unreliable, but optimized magnetization and feedforward voltages eventually enabled a reproducible reversed-B_T startup reference.

To realize long-pulse and high-confinement ($H_{98} \geq 1.5$) plasma operation, a joint research activity between DIII-D and KSTAR was newly initiated in 2024, focusing on high poloidal beta scenarios accompanied by large-radius internal transport barrier (ITB). As a preparatory work, a high poloidal beta scenario tailored for KSTAR was developed and tested on DIII-D, considering KSTAR's constraints. The principal constraints considered for KSTAR included plasma shape, delayed diverting timing, a slower plasma current ramping rate, and marginal heating power, with the latter two identified as particularly critical. Experiments on KSTAR aimed at realizing high poloidal beta plasmas with large-radius ITBs were conducted. Accordingly, additional operational constraints were imposed to minimize W impurity effects; nevertheless, promising initial results were obtained. Based on the DIII-D-developed scenario, the initial phase ($t \leq 2.0$ s) employed ~4.0 MW of NBI heating, successfully achieving an L/H transition at ~1.0 s. Subsequently, during the main heating phase, up to ~8.0 MW of NBI power was applied to trigger ITB formation and sustain high-performance plasma. Density feedback control was applied at $t \approx 1.8$ s to reach $f_{GW} \approx 0.7$, with the expectation of achieving synergistic improvements. However, in contrast to DIII-D, KSTAR performance metrics such as plasma beta exhibited a pronounced and negative sensitivity to gas fuelling. Specifically, low initial plasma density was shown to hinder the L/H transition and negatively affect early plasma performance. As shown in Fig. 2, plasma performance remained relatively low until ~6.0 s under density feedback control, but dramatically recovered once feedback was turned off. Analysis of ion temperature and rotation profiles confirmed that the beam blip at ~5.0 s acted as a positive perturbation, facilitating ITB formation in the ion temperature channel. The dramatic improvement in performance observed after density feedback was turned off ($t \approx 6.0$ s) was fundamentally attributed to pedestal enhancement.

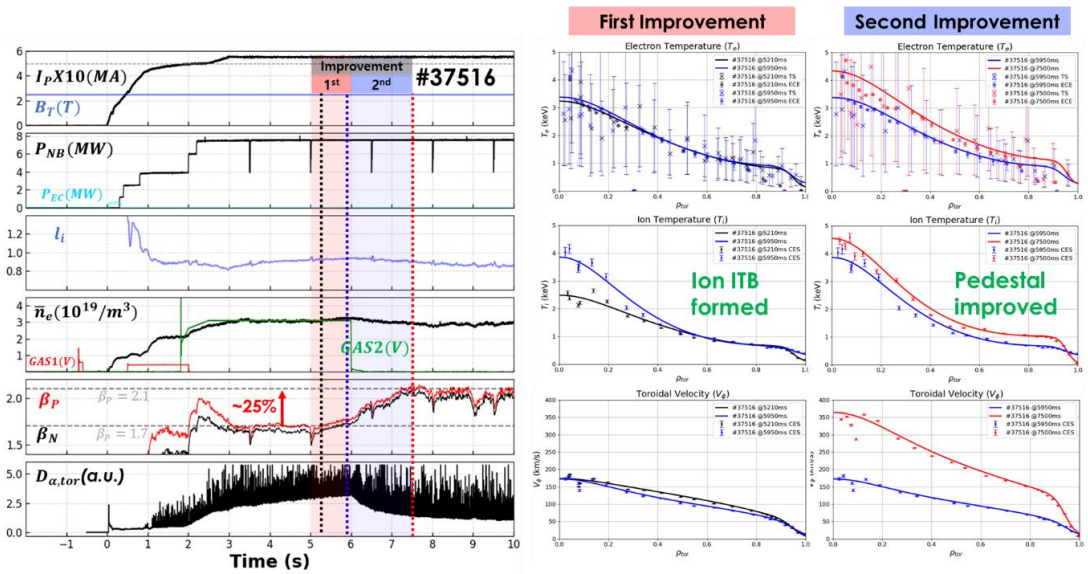

FIG 6. The first result of high poloidal beta scenario with large-radius ITB at KSTAR. A marginal ITB was achieved, triggered by a perturbation such as NBI modulations.

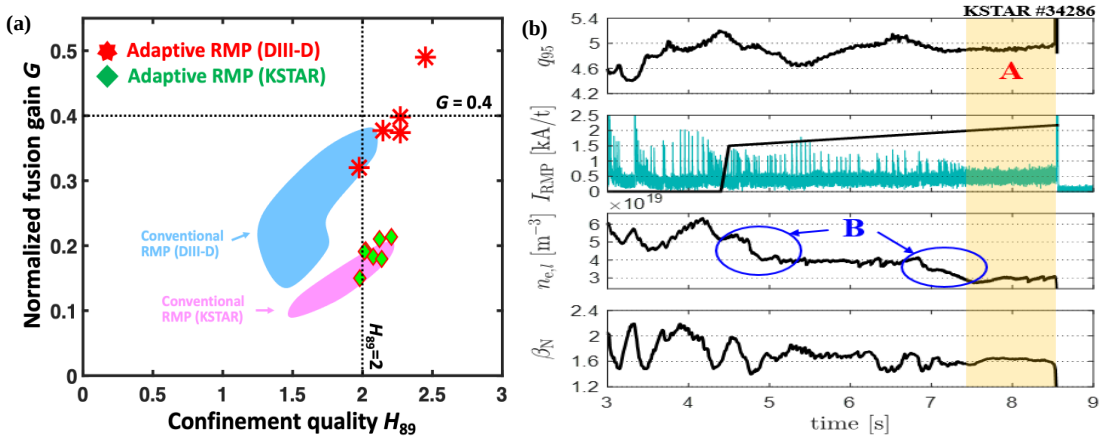

FIG 7. (a) Performance comparison of ELM-suppressed discharges in DIII-D and KSTAR tokamaks. The dashed lines indicate the ITER-relevant level. (b) Time evolutions of q_{95}, RMP current amplitude (I_{RMP}), line-averaged density ($n_{e,l}$), and β_N in the KSTAR RMP ELM suppression experiment wuth W-diveror. A (in red) denotes suppression phase, while B (in blue) represents two step density pump-out process.

Several ELM-free scenarios based on I-mode, QH-mode, IPD and ECCD-driven mode destabilization approaches are demonstrated successfully. Notice that KSTAR I-mode is an enhanced confinement ELM-free mode in anextremely low-density plasma regime (~ 1.0 x 10^{19} m^{-3}). Recently, I-mode operation have been expanded toward higher density regime by optimizing density and NBI power time traces. The plasma density was increased through gas puffing before the application of additional NBI power in the reference I-mode shot, resulting in a good I-mode in a higher density regime (~ 1.5 x 10^{19} m^{-3}).

4. IMPLEMENTATION OF CONTROL SCHEMES

Control schemes to avoid critical events were tested on new divertor environments. Recently, the real-time integrated RMP scheme [14], which leverages optimized 3D spectrum [15] and real-time adaptive ELM control, has been significantly upgraded for new W-divertor compatible shape and tested successfully in KSTAR 3D magnetic field experiments. The integrated scheme can also trigger the n=1 RMP at the L-H transition timing using the real-time ML classifier [16]. This scheme has been implemented both in the KSTAR and DIII-D tokamaks to consistently achieve ITER-relevant core confinement quality without harmful ELM crashes, as shown in FIG 7(a)[17]. In the new W monoblock-type lower divertor environment, ELM suppression by n=1 RMP has been achieved, which shows the characteristic two-step density pump-out process in the access to the ELM suppression phase (FIG 7(b)) identified in previous RMP experiments in the carbon wall. However, we have also observed that the ELM suppression is not reliable enough to ensure its sustainment for KSTAR long-pulses, with low reproducibility compared to the previous results from carbon-wall conditions. Moreover, detailed analysis of the pedestal profile data during the suppression (-like) phase shows that the pedestal ion temperature and the plasma toroidal rotation with W-divertor are significantly lower than those with C-divertor, which could contribute to the less robust suppression results under the W divertor conditions. Thus, this experimental observation might imply a significant wall recycling (or impurity) impact associated with W wall retention (i.e., low fuel retention), requiring a further detailed study on securing complete and stable RMP-driven ELM suppression in the W divertor environment.

Physics-based disruption event characterization and forecasting (DECAF) research [18] determines the relation of physical events leading to disruption. The first real-time demonstration of disruption avoidance by DECAF was produced on KSTAR by connecting DECAF events to control actuators and applying event feedback. The number of DECAF Events is now significantly expanded (two in 2022) to eight, that examine various physical phenomena in their first real-time incarnation, including plasma current anomalies [19], vertical instability [20], an upgraded capability of predicting and forecasting MHD mode-locking [2], and impurity radiative collapses. The critical new multi-Event feedback capability leverages the high accuracy of DECAF Events [19] now cueing device actuators to produce disruption avoidance. FIG 8(a) shows a compilation of results using multiple Events illustrating examples of disruption prediction, avoidance, and optimization. The DECAF approach to disruption prediction is multi-tiered to ensure that sufficient time between the critical (Level 3) prediction warning and the disruption is sufficient for disruption mitigation in ITER (nominally 50 ms). To produce an earlier disruption

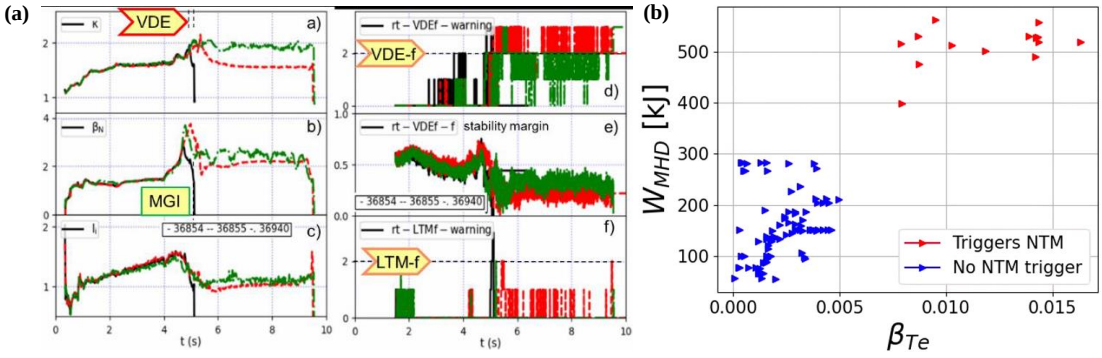

FIG 8. (a) Disruption avoidance and optimization with DECAF VDE-f Event feedback using plasma shape control and LTM-f Event active; disruption mitigation triggers by VDE Event when feedback is disabled. (b) Separation of Te collapses triggering NTM-induced disruptions for KSTAR TEC Event.

warning, a VDE forecaster Event (VDE-f) was created based on a vertical force balance model including the applied equilibrium field, 2-D plasma current, and eddy currents [20]. This Event can activate a variety of KSTAR control actuators including a controller that can modify the plasma shape in real-time [21]. The target plasmas produced high transient normalized beta, β_N up to 3.9. Once VDE-f reaches the Level 2 warning, the real-time VDE-f Event stability calculation is compared to a target value of 1.3 to produce a target error for proportional gain feedback. The resultant Event feedback control signal alters the plasma elongation for disruption avoidance. Due to the physics understanding and database analysis that DECAF Events provide, plasma experiments demonstrated the capability and provided physics understanding immediately following the activation of Event

feedback components. New and updated DECAF Events were recently added with feedback capabilities including an LTM-f Event that now actuates an $n = 1$ rotating field to avoid mode locking. This Event feedback was active, but not triggered as warnings were transiently at or below the proximity Level. These new DECAF Events were run simultaneously, including VDE-f actuating both shaping control and ECH/ECCD, LTM-f actuating an $n = 1$ rotating field, and VDE disruption prediction set to trigger MGI for plasma shutdown. Other new Events have been studied using the tokamak databases and each have warning levels that correlate with plasma disruptions including a generalized capability to diagnose electron temperature collapses (TEC) that provide early disruption prediction by ~ 0.7s and good condition separation (FIG 8(b)).

Another approach for disruption avoidance using a data-driven neural network during high-current MA-level experiments was developed [22]. The system utilized massive gas injection (MGI) as the primary mitigation method, which was confirmed to be effective in both MA plasma development and high-density operation sessions. During these experiments, the system accurately predicted disruptions stemming from unexpected H- to L-mode transitions and critical density thresholds, enabling timely mitigation. Quantitative analysis showed that

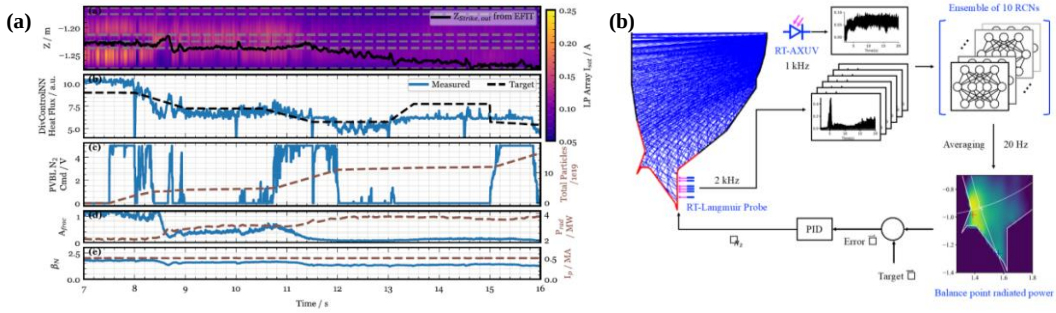

FIG 9. (a) Demonstration of real-time divertor detachment control in KSTAR using a surrogate model (DivControlNN). Left: schematic of the multi-modal prediction model trained on a large UEDGE simulation database. Right: experimental validation showing controlled J_{sat} and heat flux via real-time nitrogen seeding, with stable impurity radiation fraction and β_N. (b) Machine learning–based control of the divertor radiation front in KSTAR. Left: control architecture combining real-time Langmuir probe (2 kHz) and AXUV (1 kHz) diagnostics with neural network predictors. Right: experimental validation showing stable control of the radiation front position across multiple discharges, with minimal impact on β_N.

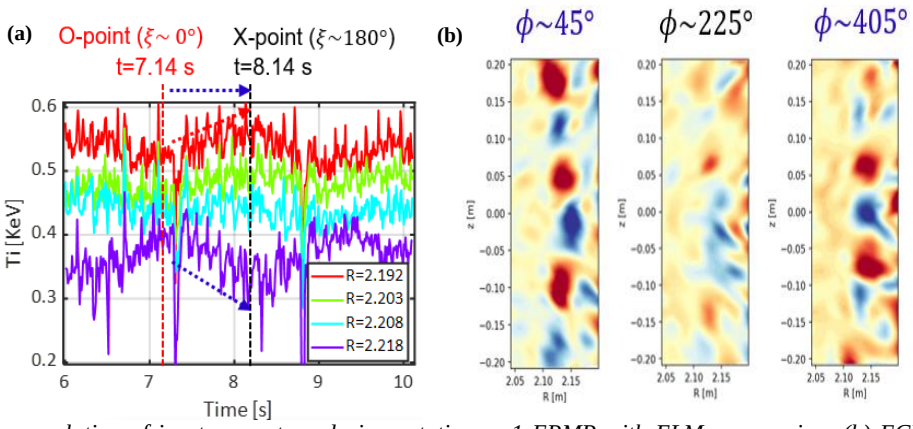

FIG 10. (a) Time evolution of ion temperature during rotating n=1 ERMP with ELM suppression. (b) ECEI data at different toroidal angles showing 3D-localized filament structure at the specific toroidal angle.

using MGI significantly reduced the impact on in-vessel components compared to normal disruptions. The safety benefits were further enhanced when MGI was combined with a rapid plasma current ramp-down.

KSTAR has advanced real-time control techniques to maintain the divertor detachment conditions. A surrogate model derived from UEDGE simulations was integrated into the plasma control system (PCS) to guide nitrogen seeding dynamically during discharges. This approach enabled precise regulation of the divertor ion saturation current (J_{sat}), maintaining target detachment levels in real time (FIG 9). Furthermore, machine learning–based controllers were developed using real-time AXUV and Langmuir probe signals, enabling direct control of the divertor radiation front location with minimal impact on β_N and core confinement. The machine learning–based controller is trained with both AXUV data, which measures total plasma radiation loss, and IRVB data, which provides two-dimensional radiation profiles. As a result, the controller can infer 2D plasma radiation structures

from AXUV measurements alone, allowing estimation and control of the radiation front position even in the absence of IRVB data. These achievements represent a crucial step toward ITER-relevant real-time impurity and detachment control.

5. INVESTIGATION ON PHYSICAL MECHANISM

In the physics study of the 3D transport and magnetic island (MI) effects, direct evidence of edge magnetic island, i.e., phase flip in signal (π difference), is observed for the first time with ELM suppression in the ion temperature (T_i) channel associated with a rotating n=1 edge localized RMP (ERMP) [23], as shown in FIG 10(a). The estimated island center is located near the pedestal top, and phase flip is only clear during the ELM suppressed phase and does not exist for the ELM mitigated phase. Therefore, the key results agree well with the predicted role of magnetic islands in RMP ELM suppression [24]. On the other hand, a 3D turbulence structure with an edge magnetic island shows that edge magnetic island leads to 3D filament-like structure localized at the specific toroidal angle, as shown in FIG 10(b). Maximum particle flux is measured at this angle, implying its role in optimizing ELM-suppression state. Besides this MI-induced particle transport effect, KSTAR also reported that when the rotating RMP is applied, edge kink-like modes are usually observed and found to cause enhanced particle transport due to the associated plasma surface displacements [25].

Control of the toroidal Alfvén eigenmode (TAE) has been demonstrated using two actuators, such as electron cyclotron current drive (ECCD) and beam-drive change, during the 2024 experimental campaign. The primary mechanism for stabilizing AEs in this study is continuum damping [26, 27]. In addition to the AE suppression experiments using the single-ECCD scan [28], local magnetic shear changes caused by scanning with the two ECCDs also demonstrate the possibility of TAE control. It is observed that a favorable combination of the adjacent ECCD directions, which increases the local magnetic shear near the AE location, can mitigate the AEs. In this result, performance (i.e., β_N (with $\beta_N > 2.5$, max 3.0) and stored energy difference (W_{MHD}-W_{DIA})) has also shown enhancement for over 5 seconds during the inward radial ECCD deposition scan.

Beam-drive reduction has also been attempted by broadening the beam-ion profile while maintaining the total NBI power. TAE-controlled discharge has been achieved with this technique when the NBI power deposit (especially the tangential beam) at the core is spread. Performance enhancement ($\beta_N > 2.4$) has also been achieved

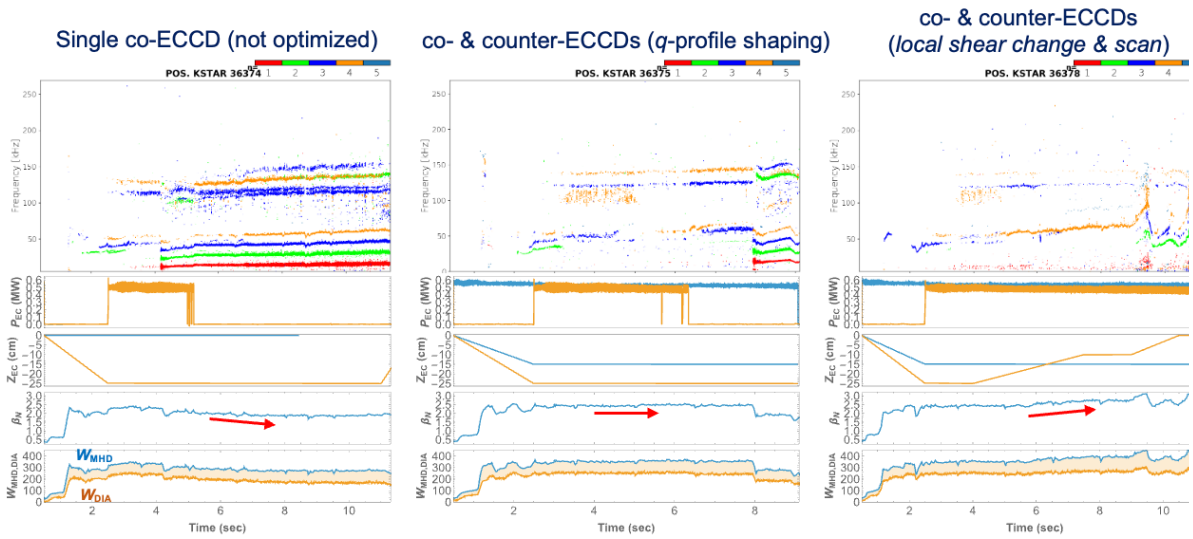

FIG 11. TAE control by the local magnetic shear change and scan using the multiple (co & counter directions) ECCD applications enhances the plasma performance. Stored energy difference ($W_{MHD} - W_{DIA}$) depicted in the bottom figures indicates the confinement enhancement of the fast-ions.

during the TAE-control phase in this experiment. A change in the beam-ion energy profile through intra-shot beam-energy control could reduce the fast-ion pressure gradient in the core region. This can have a positive effect, allowing mode damping to overcome the mode drive. These results suggest that in-shot beam-drive adjustments can support ECCD-assisted TAE control when the primary damping mechanism alone is not enough to stabilize the TAEs. However, combining NBI with higher injection power is necessary to evaluate its effectiveness under higher beam-drive conditions. It is also observed that fast-ion loss is significantly reduced when the AEs are controlled and βN is increased, as reported in a previous investigation [28]. In experimental observations, the fast-ion distribution is sensitive to the AE resonance condition in phase-space. This suggests that controlling the fast-ion phase-space is crucial for managing energetic-particle instabilities and optimizing fast-ion populations in future experiments.

Complicated behavior of transport in the ITG-near-marginal regime of KSTAR plasmas has been investigated [29]. The transport in the near-marginal regime poses challenges for transport modelling due to mesoscopic structures. In KSTAR plasmas, the near-marginal regime is characterized by a marginal ITG drive and the scale-free ballistic transport events. These transport events can be confined by mesoscopic transport barriers, the E ×B staircase, until the barriers are dissipated or destroyed. Corrugated temperature profile and reduced turbulence correlation length have been identified using the ECEI and BES diagnostics. Experiments in KSTAR, HL-3, and DIII-D investigated the formation mechanism and the stability of the E×B staircase, consistently revealing similar transport events and the hint of the mesoscopic transport barriers as shown in FIG 12.

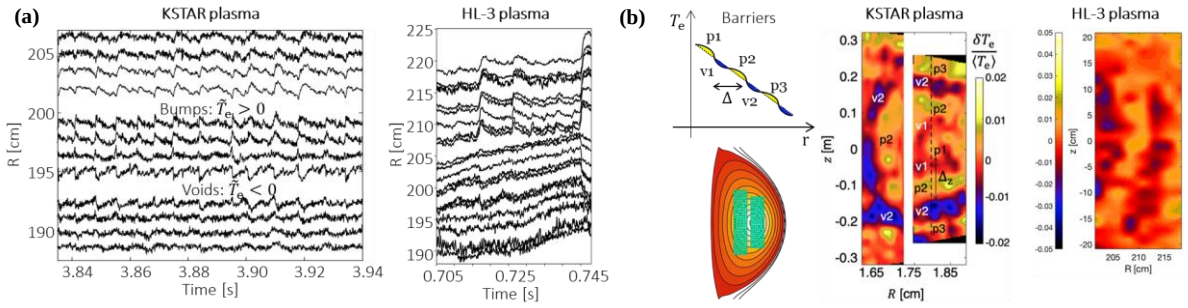

FIG 12. (a) The scale-free transport events in KSTAR and HL-3 plasmas. The pair creation and opposite propagation of temperature bumps and voids are shown. (b) Mesoscopic transport barriers in KSTAR and HL-3 plasmas

The coupled influence of the heating power ratio between electron cyclotron heating (ECH) and neutral beam injection (NBI) on turbulence and transport in H-mode plasmas is being investigated. Substituting NBI with ECH consistently reduced toroidal rotation and led to an inversion of the electron-to-ion temperature ratio (T_e/T_i) on axis, primarily due to a substantial decrease in T_i while T_e was only weakly affected. In addition, an increase in density fluctuation measured by the collective scattering system [30] was observed with rising T_e/T_i. This result is consistent with the destabilization of ion scale turbulence such as ion temperature gradient mode and trapped electron mode with increasing T_e/T_i. Possible changes in electron scale turbulence, such as electron temperature gradient mode, should also be considered, as they can contribute to the stiff T_e profile. Variations in the E×B shearing rate associated with the heating ratio scan are expected to influence the saturation levels of turbulence and transport. Further analysis and modeling are planned to quantify how the heating ratio affects turbulence and transport.

6. SUMMARY AND OUTLOOK

The 2023-2024 KSTAR experimental campaigns have marked an important transition toward reactor-relevant operation with the commissioning of the W monoblock divertor. Systematic studies revealed the substantial impact of tungsten impurities on core plasma performance, confirming that impurity control remains one of the most critical challenges for future devices. Dedicated scenario development, including delayed NBI heating, boron powder injection, and advanced gas-puffing strategies, has proven effective in mitigating impurity accumulation and preventing performance degradation. These results validate the compatibility of tungsten-facing components with high-performance scenarios, while also highlighting the need for continuous improvement in impurity transport understanding and control techniques.

The development and extension of advanced scenarios demonstrated that KSTAR can access a wide operational space in the tungsten environment. Collaborative efforts with DIII-D have been instrumental in tailoring high poloidal beta scenarios to KSTAR constraints, successfully demonstrating ITB formation in high-density plasmas. Although confinement improvements were not as strong as in DIII-D, these results provide a foundation for further optimization, particularly in balancing pedestal performance with impurity control. The importance of real-time control in future tokamaks will continue to grow. Upgraded RMP schemes, disruption forecasting with DECAF, and surrogate-model-based divertor detachment control represent major steps toward ITER-relevant plasma management. Machine-learning-based diagnostics and controllers further expanded the scope of real-time plasma optimization, opening pathways for integration of AI-assisted control in future campaigns. Beyond scenario and control development, KSTAR contributed significantly to advancing the physics basis for burning plasmas. Experiments provided new insights into turbulence, transport near marginal stability, magnetic island–induced transport, and fast-ion interactions with Alfvén eigenmodes. These studies not only benchmark transport models but also reveal the interplay of multi-scale phenomena critical to confinement optimization in tungsten-wall environments.

Looking forward, KSTAR will pursue several key directions. The transition to a full-tungsten wall and ITER-aligned real-time control framework will establish a more stringent test bed for reactor-relevant operation. Planned hardware upgrades, including expanded heating/current-drive capability and enhanced diagnostics, will further support the realization of steady-state, non-inductive scenarios. Continued international collaboration will accelerate the development of optimized advanced scenarios, providing essential inputs for ITER and DEMO. In summary, the KSTAR tungsten-divertor campaigns have demonstrated both the challenges and opportunities of operating under reactor-relevant plasma wall conditions. By integrating scenario innovation, advanced control, and physics discovery, KSTAR is rapidly consolidating its role as a leading experimental platform for developing the operational strategies required to achieve steady-state burning plasmas.

ACKNOWLEDGEMENTS

This research was supported by the R&D Program of "High Performance Tokamak Plasma Research & Development (EN2501-16)" through the Korea Institute of Fusion Energy (KFE) funded by Korea Ministry of Science and ICT (MSIT).

REFERENCES

[1] PARK, H.K. et al, Nucl. Fusion **59** (2019) 112020.
[2] KO, W.H et al, Nucl. Fusion **64** (2024) 112010

[3] LEE, H. et al, Phys. Plasma **29** (2022) 022504
[4] DOMINSKI, J. et al, Nucl. Fusion **65** (2025) 016003
[5] SCHAMIS, H. et al, Nucl. Fusion **65** (2025) 086037
[6] PARK, J.M. et al, "Long Pulse High Li Steady State Scenario On KSTAR", 2257, 29th IAEA FEC, London, UK, 2024
[7] NA, Y.S. et al, Nucl. Fusion **60** (2020) 086006
[8] CHUNG, J. et al, Nucl. Fusion **61** (2021) 126051
[9] HAN, H, PARK, S.J. et al, Nature **609** (2022) 269
[10] KIM, H.-S. et al, Nucl. Fusion **64** (2024) 016033
[11] LEE, Y.H. et al, Nucl. Fusion **63** (2023) 126032
[12] KIM, B. et al, Nucl. Fusion **63** (2023) 126013
[13] CHUNG, J. et al, "Assessing the Impact of the Tungsten Environment on High-Performance Scenarios in KSTAR: Initial Results", We1A-1, 3rd International Fusion and Plasma Conference, Seoul, Korea, 2024
[14] KIM, M. et al, Nucl. Fusion **63** (2023) 086032
[15] YANG, S.M. et al, Nature Commun. **15** (2024) 1275
[16] SHIN, G. et al, Nucl. Fusion **62** (2022) 026035
[17] KIM, S. K. et al, Nature Commun. **15** (2024) 3990
[18] SABBAGH, S.A. et al, Phys. Plasmas **30** (2023) 032506.
[19] ZAMKOVSKA, V., et al., Nucl. Fusion **64** (2024) 066030
[20] TOBIN, M., et al., Plasma Phys. Control. Fusion **66** (2024) 105020
[21] BARR, J., et al., Nucl. Fusion **61** (2021) 126019
[22] LEE, J. et al, Nucl. Fusion **65** (2025) 056040
[23] YANG, S.M. et al, "Observation of edge magnetic islands and 3D turbulence structure during RMP ELM suppression," IAEA, China (2025), accepted
[24] WILENSDORFER, M. et al, Nat. Phys. **20** (2024) 1980
[25] LEE, J.K. et al, Phys. Plasmas **32** (2025) 012303
[26] Zonca F. and Chen L. 1992 *Phys. Rev. Lett.* **68** 592–5
[27] Zonca F. and Chen L. 1993 *Phys. Fluids* B **5** 3668
[28] KIM, J. et al, Nucl. Fusion **62** (2022) 026029
[29] CHOI, M.J. et al, Plasma Phys. Control. Fusion **66** (2024) 065013
[30] LEE, W. et al, Phys. Plasmas **63** (2021) 035003